NJC

Accepted Manuscript

This is an *Accepted Manuscript*, which has been through the Royal Society of Chemistry peer review process and has been accepted for publication.

Accepted Manuscripts are published online shortly after acceptance, before technical editing, formatting and proof reading. Using this free service, authors can make their results available to the community, in citable form, before we publish the edited article. We will replace this *Accepted Manuscript* with the edited and formatted *Advance Article* as soon as it is available.

You can find more information about *Accepted Manuscripts* in the Information for Authors.

Please note that technical editing may introduce minor changes to the text and/or graphics, which may alter content. The journal's standard Terms & Conditions and the Ethical guidelines still apply. In no event shall the Royal Society of Chemistry be held responsible for any errors or omissions in this *Accepted Manuscript* or any consequences arising from the use of any information it contains.

ROYAL SOCIETY OF CHEMISTRY

www.rsc.org/njc

Improved Electrochemical Properties of $(1-x)LiFePO_4 \cdot xLi_3V_2(PO_4)_3/C$ Composites Prepared by Novel Sol-gel Method

*Yuanchang Si, Zhi Su *, Yingbo Wang, Ting Ma, Juan Ding*

(College of Chemistry and Chemical Engineering, Xinjiang Normal University, Urumqi, 830054, Xinjiang, China)

Abstract

In this study, $(1-x)LiFePO_4 \cdot xLi_3V_2(PO_4)_3/C$ (x=0, 0.1, 0.2, 0.3, 0.4, 0.5 and 1) composite cathode materials are synthesized using $CH_3COOLi \cdot 2H_2O$, $Fe(CH_3COO)_2 \cdot 4H_2O$, V_2O_5, and H_3PO_4 as starting materials with N,N-dimethyl formamide as a dispersing agent using a novel sol-gel method. The structure, morphology, and electrochemical properties of the composites are characterized by X-ray diffraction (XRD), transmission electron microscopy (TEM), X-ray photoelectron spectroscopy (XPS), cyclic voltammetry (CV), electrochemical impedance spectroscopy (EIS), and charge-discharge measurements. XRD patterns of the compound indicate the coexistence of $LiFePO_4$ and $Li_3V_2(PO_4)_3$. Compared to pristine $LiFePO_4$ and $Li_3V_2(PO_4)_3$, the composite materials exhibit smaller particle size, which can facilitate Li^+ extraction and insertion, thereby leading to an improvement in the electrochemical properties. Among all the composites synthesized, $0.8LiFePO_4 \cdot 0.2Li_3V_2(PO_4)_3/C$ exhibits the best electrochemical performance with an initial specific discharge capacity of 158.7 $mAh \cdot g^{-1}$ at 0.1 C in the voltage range of 2.5-4.3 V. When the current rate is increased to 5 C and 10 C, the capacity of $0.8LiFePO_4 \cdot 0.2Li_3V_2(PO_4)_3/C$ is retained at 125.8 and 110.8 $mAh \cdot g^{-1}$, respectively, indicating the cycling stability of the composite.

Keywords: composite material; sol-gel; nanoparticle; electrochemical properties

∗Corresponding author. Tel.: +86- 991-4332683; fax: +86-991-4332683.

E-mail address: suzhixj@sina.com (Z. Su).

New Journal of Chemistry Accepted Manuscript

Introduction

Polyanion materials have drawn much attention as cathode materials for lithium-ion batteries, owing to their thermal stability and superior safety [1-3]. Among the various polyanion materials, $LiFePO_4$, which has particular advantages such as low cost, superior thermal stability, relatively high theoretical capacity (170 $mAh \cdot g^{-1}$), environmental friendliness, and high safety, has been intensely studied since 1997[4-7]. However, it suffers from poor electronic conductivity (10^{-7}-10^{-9} $S \cdot cm^{-1}$) and requires a stringent synthesis methodology, which restrict it from being used in large-scale applications such as in electric vehicles and other devices that demand high power [8-9]. Many measures have been taken to overcome these problems associated with $LiFePO_4$, and several strategies such as carbon coating [10-11], reducing particle size [12-13], ion doping [14-15], and addition of metals [16-17] have been implemented. Besides $LiFePO_4$, another polyanion phosphate, $Li_3V_2(PO_4)_3$, is also a promising cathode material and has also received intense attention because of its stable framework, superior ionic mobility, high reversible capacity, and relatively high operating voltage [18-20]. $Li_3V_2(PO_4)_3$, with its three-dimensional framework, contains three independent lithium sites and allows fast ion migration [21-23].

However, the main disadvantage of both $LiFePO_4$ and $Li_3V_2(PO_4)_3$ is their low electronic conductivity, which limits their electrochemical properties at high rates. At present, there are some reports available on $(1-x)LiFePO_4 \cdot xLi_3V_2(PO_4)_3$/C composite materials [24-34]. For example, Yang [24] et al. synthesized $LiFePO_4 \cdot Li_3V_2(PO_4)_3$/C and found that the conductivity of $LiFePO_4$ was greatly enhanced by the introduction of $Li_3V_2(PO_4)_3$. Ma [25] et al. studied the effect of the addition of $Li_3V_2(PO_4)_3$ to $LiFePO_4$. Zheng [27] et al. synthesized $LiFePO_4 \cdot Li_3V_2(PO_4)_3$, which showed good electrochemical performance. The discharge capacity of this compound was found to be about 116 $mAh \cdot g^{-1}$ at 3 C. Xiang [31] et al. prepared a composite via carbon thermal reaction, which exhibited a discharge capacity of 125 $mAh \cdot g^{-1}$ after 150 cycles. Zheng [32] et al. synthesized pure $LiFePO_4$, $Li_3V_2(PO_4)_3$, and two-component powders $xLiFePO_4 \cdot yLi_3V_2(PO_4)_3$ through a chemical reduction and lithiation method,

New Journal of Chemistry Accepted Manuscript

and $xLiFePO_4 \cdot yLi_3V_2(PO_4)_3$ material showed better electrochemical performance compared with individual $LiFePO_4$ and $Li_3V_2(PO_4)_3$. A series of $xLiFePO_4 \cdot yLi_3V_2(PO_4)_3$/C cathode materials are synthesized by using a sol spray drying method by Wu [33] et al., and 3LFP·LVP/C possesses the best comprehensive performance. All of the above studies confirm that the electrochemical properties of $LiFePO_4$, especially at high current rates, can be greatly improved by adding $Li_3V_2(PO_4)_3$. To the best of our knowledge, $Li_3V_2(PO_4)_3$ exhibits three voltage plateaus around 3.6, 3.7 and 4.1 V in the voltage range of 2.5-4.3 V, which are all higher than the voltage plateau exhibited by $LiFePO_4$ at 3.5 V [4, 35]. This implies that adding vanadium may enhance the power density of $LiFePO_4$, and further enhance the electrochemical performance.

In this study, a series of $(1\text{-}x)LiFePO_4 \cdot xLi_3V_2(PO_4)_3$/C composites materials were synthesized by a new sol-gel method with N,N-dimethyl formamide (DMF) as the solvent, which can control the particle size of the composite material. The sol-gel method is a simpler, less-energy intensive and low-cost method compared to the other methods that have been adopted.

Experimental

Synthesis

The $(1\text{-}x)LiFePO_4 \cdot xLi_3V_2(PO_4)_3$/C composites were prepared by the sol–gel method with DMF as the solvent. All the reagents were of analytical grade. Stoichiometric ratios of $CH_3COOLi \cdot 2H_2O$, $Fe(CH_3COO)_2 \cdot 4H_2O$, V_2O_5, H_3PO_4, and glucose were employed as the starting materials for the sol-gel process. Glucose was used as the carbon source and as a reducing agent. Firstly, V_2O_5 was added to 5 mL H_2O_2 (30 wt. %) and magnetically stirred to form red-brown V_2O_5 hydrogels. Subsequently, 50 mL of DMF was added to this mixture, following which $CH_3COOLi \cdot 2H_2O$ and $Fe(CH_3COO)_2 \cdot 4H_2O$ in the stoichiometric ratio were dissolved in the solution. Next, glucose and H_3PO_4 (85 wt. %) were dissolved in 30 mL DMF. The two solutions were then mixed to obtain a sol, which was heated at 80 ºC until a gel was formed and subsequently dried in a vacuum oven at 40 ºC. The as-obtained

New Journal of Chemistry Accepted Manuscript

xerogel was pre-calcined at 300 ºC for 3 h, followed by final calcination at 700 ºC for 12 h under argon atmosphere in a tube furnace. This procedure resulted in the production of (1-x)$LiFePO_4 \cdot xLi_3V_2(PO_4)_3$/C (x=0, 0.1, 0.2, 0.3, 0.4, 0.5 and 1) composite materials.

Characterization

The phase identity of the samples was analyzed by X-ray diffraction (XRD, Bruker D2) using Cu Kα radiation. The diffraction data were collected in the step mode over the angular range (2θ) of 10-70° with a step size 0.02° at 30 kV and 10 mA. Scanning electron microscopy (SEM, Germany Zeiss Supra 55VP) images were collected at an acceleration voltage of 20 kV. Transmission electron scanning electron microscopy (TEM, FEI Tecnai 20)) images of the samples were collected at an acceleration voltage of 200 kV. The valences of iron and vanadium ions were detected by an X-ray photoelectron spectrometer (XPS, PHI-5300 ESCA) equipped with an Al Kα achromatic X-ray source.

For the electrochemical measurements, the cathode was fabricated by mixing 80 wt. % active material, 15 wt. % acetylene black, and 5 wt. % polytetrafluoroethylene (PTFE) in deionized water. The obtained slurry was coated on an Al foil, and dried at 80 °C for 12 h under vacuum. The loading density of the active material was approximately 2-3 $mg \cdot cm^{-2}$. The electrolyte consisted of 1 M $LiPF_6$ in a mixture of ethylene carbonate/dimethyl carbonate (EC/DMC) (1:1 by volume). The electrochemical capacity and cycle performance of the electrodes were tested using a battery test system (LAND Wuhan, China CT-2001A) between 2.5 and 4.3 V at room temperature.

Cyclic voltammetry (CV) and electrochemical impedance spectroscopy (EIS) measurements were carried out with an electrochemical workstation (China Tianjin, LK2005A). The CV curves were recorded in the potential range of 3.0-4.3 V at a scan rate of 0.1 $mV.s^{-1}$ at room temperature, whereas the EIS data were recorded in the frequency range of 1 Hz to 100 kHz.

New Journal of Chemistry Accepted Manuscript

Results and discussion

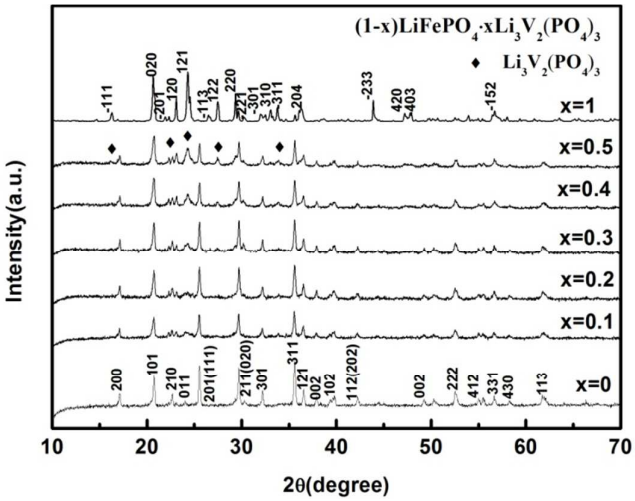

Fig. 1 XRD patterns of (1-x)$LiFePO_4 \cdot xLi_3V_2(PO_4)_3$/C samples.

Table 1

Carbon contents of as-prepared materials.

Sample(1-x)$LiFePO_4 \cdot xLi_3V_2(PO_4)_3$/C	x=0	x=0.1	x=0.2	x=0.3	x=0.4	x=0.5	x=1
Carbon content (wt%)	4.7	4.8	4.6	4.8	4.5	4.7	4.6

The crystal structures of the (1-x)$LiFePO_4 \cdot xLi_3V_2(PO_4)_3$/C samples synthesized by the sol-gel method were determined by powder XRD and the results are shown in Fig. 1. The sharp peaks in the patterns indicate that all the samples are adequately crystalline. For the samples where x=0 and 1, all the diffraction peaks correspond to olivine $LiFePO_4$ (JCPDS 40-1499) and monoclinic $Li_3V_2(PO_4)_3$ (JCPDS 47-0107), respectively. On the other hand, the diffraction peaks of (1-x)$LiFePO_4 \cdot xLi_3V_2(PO_4)_3$/C (where x=0.1, 0.2, 0.3, 0.4, and 0.5) are composed of both the $LiFePO_4$ and $Li_3V_2(PO_4)_3$ phases without any impurity. With increase in the amount of vanadium, the peaks corresponding to monoclinic $Li_3V_2(PO_4)_3$ become obvious. In addition, although glucose was used as the carbon source, a carbon phase is not detected, indicating that the carbon generated from glucose is amorphous and its presence does not influence the crystal structure of (1-x)$LiFePO_4 \cdot xLi_3V_2(PO_4)_3$[36]. In addition, the carbon contents in all (1-x)$LiFePO_4 \cdot xLi_3V_2(PO_4)_3$/C composites were

New Journal of Chemistry Accepted Manuscript

measured by elemental analysis, as shown in Table 1. The contents of residual carbon in all as-prepared samples are similar, indicating that the different electrochemical performances are attributed to the different ratio between $LiFePO_4$ and $Li_3V_2(PO_4)_3$ [37].

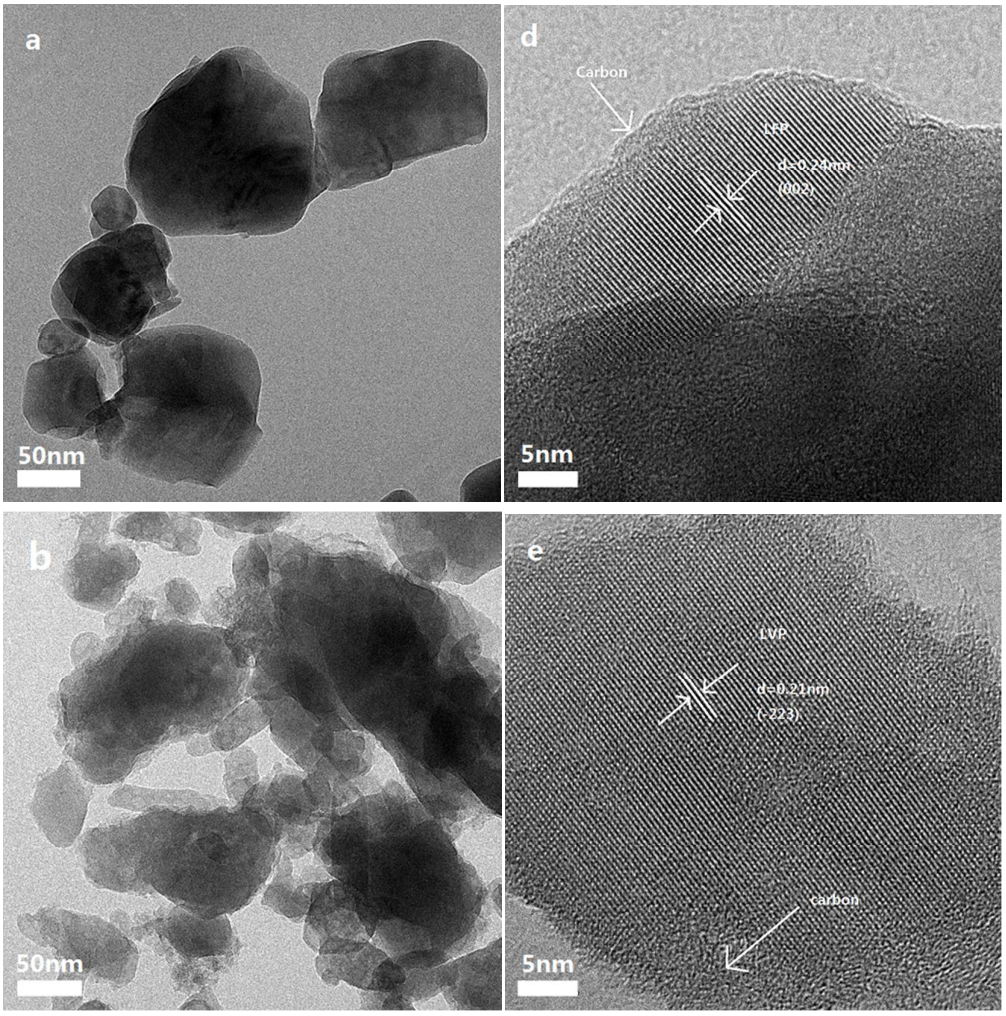

New Journal of Chemistry Accepted Manuscript

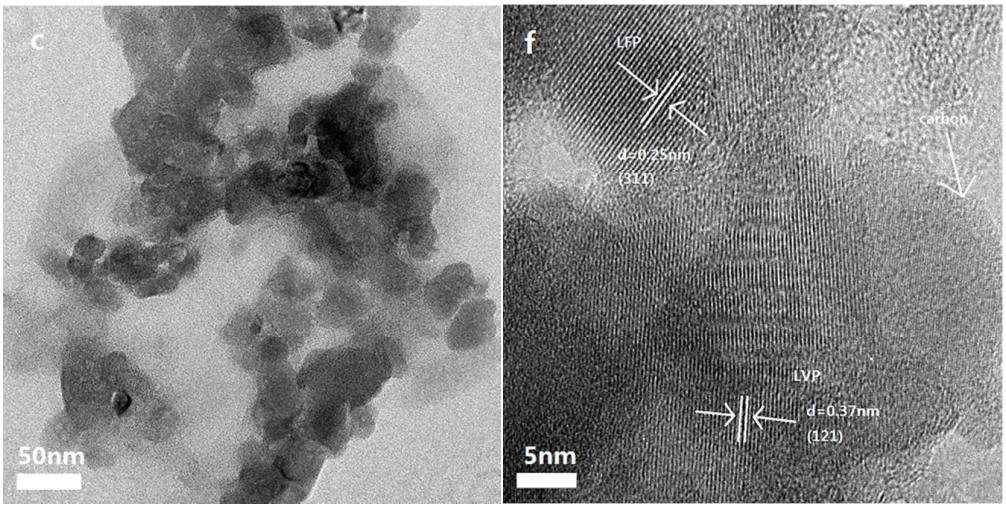

Fig. 2 TEM and HRTEM images of (a)(d) $LiFePO_4$/C, (b)(e) $Li_3V_2(PO_4)_3$/C and (c)(f) $0.8LiFePO_4 \cdot 0.2Li_3V_2(PO_4)_3$/C.

TEM images of the $(1-x)LiFePO_4 \cdot xLi_3V_2(PO_4)_3$/C composites with x values of 0, 1, and 0.2 are shown in Fig. 2a-c, respectively. As shown, all the three samples exhibit similar morphologies with irregular particles. In addition, some large particles are also detected, and the prepared particles have been uniformly coated with carbon. Fig. 2a shows that $LiFePO_4$C consists of relatively larger particles with grain diameter in the range of 30-150 nm. On the other hand, $Li_3V_2(PO_4)_3$/C has agglomerated clusters consisting of small particles as well as some large particles, as shown in Fig. 2b. However, $0.8LiFePO_4 \cdot 0.2Li_3V_2(PO_4)_3$/C (Fig. 2c) shows relatively uniform small particles with grain diameter of 30-50 nm. According to a previous report by our group, DMF not only acts as a chelating agent assisting in the formation of the gel, but can also control the particle size of the product by forming complexes with metal ions. On the other hand, the addition of H_3PO_4 results in the slow release of metal ions from the complex, to participate in the reaction [38].

Fig. 2d-f show the HRTEM images of $LiFePO_4$/C, $Li_3V_2(PO_4)_3$/C, and $0.8LiFePO_4 \cdot 0.2Li_3V_2(PO_4)_3$/C, respectively. It can be seen from Fig. 2d that $LiFePO_4$/C exhibits regular lattice fringes of the (002) crystalline plane with a

New Journal of Chemistry Accepted Manuscript

measured d-spacing value of 0.24 nm. On the other hand, the visible legible lattice fringes with d-spacing of 0.21 nm shown in Fig. 2e, correspond to the (-223) plane of $Li_3V_2(PO_4)_3$/C. In Fig. 2f, the HRTEM image of $0.8LiFePO_4 \cdot 0.2Li_3V_2(PO_4)_3$/C shows evidence of two lattices. One of these can be associated with the lattice fringe of $LiFePO_4$ (d-spacing of 0.25 nm, lattice plane (311)), whereas the other, whose d-spacing is measured to be 0.37 nm, is consistent with the fringe spacing values of the (121) plane of $Li_3V_2(PO_4)_3$/C. This result demonstrates that the as-prepared materials form a composite composed of $LiFePO_4$-$Li_3V_2(PO_4)_3$/C [39]. The particles of all the samples are found to be wrapped in nanoscale carbon webs, which can offer a good electronic conduction network for the active materials [40].

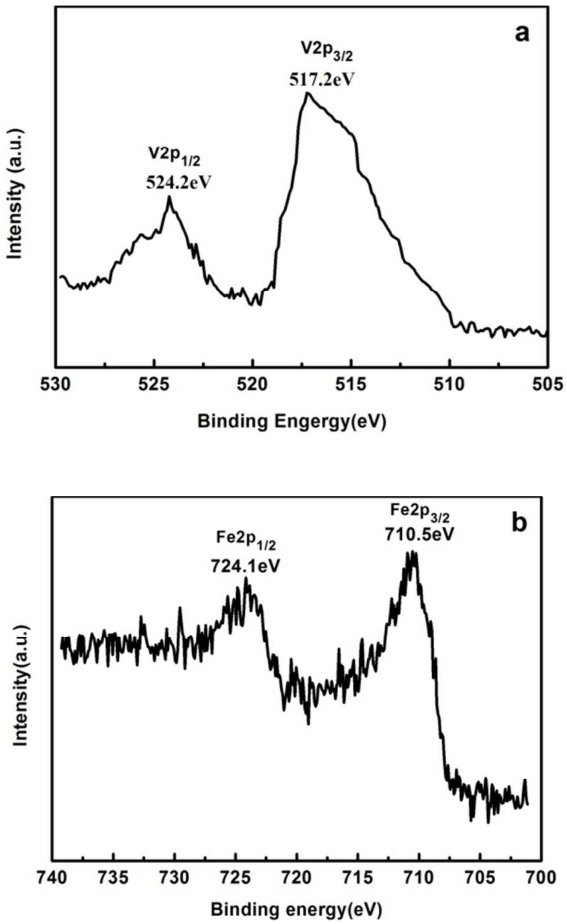

Fig. 3 XPS spectra of V2p (a) and Fe2p (b) in $0.8LiFePO_4 \cdot 0.2Li_3V_2(PO_4)_3$/C.

New Journal of Chemistry Accepted Manuscript

The valence states of Fe and V in the $0.8LiFePO_4 \cdot 0.2Li_3V_2(PO_4)_3/C$ composite were conducted through XPS. In Fig. 3a, the XPS spectra of V2p showed two peaks with binding energy of 524.2 eV and 517.2 eV, which can be assigned to $V2p_{1/2}$ and $V2p_{3/2}$. The binding energies of both peaks matched well with that observed in V_2O_3 [41] and $Li_3V_2(PO_4)_3$ [42], indicating that the oxidation states of V is +3. It can be found from Fig. 3b, the XPS spectrum of Fe2p can be split into two spectra $Fe2p_{1/2}$ and $Fe2p_{3/2}$ with binding energy of 724.1eV and 710.5 eV. The result shows that the valence of Fe in the composite is +2[43].

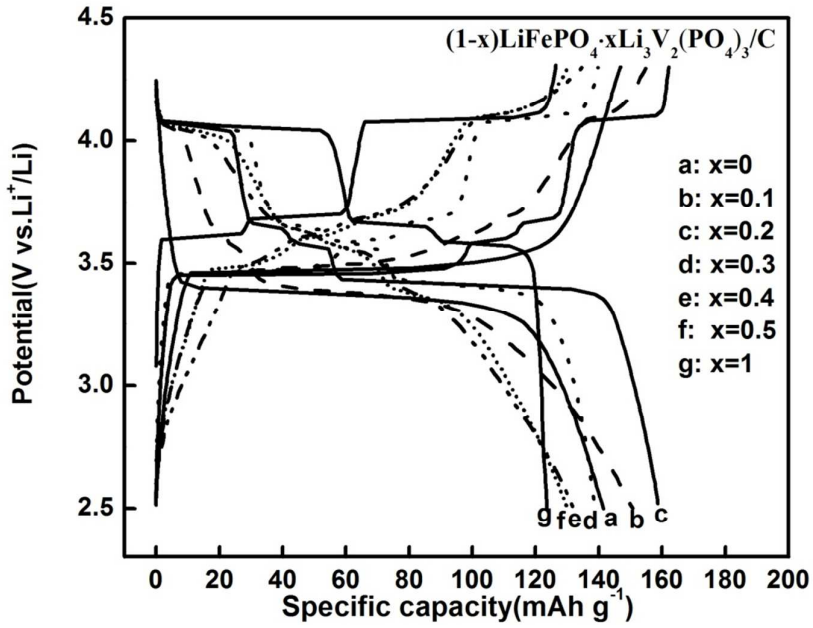

Fig. 4 Initial charge-discharge curves of $(1-x)LiFePO_4 \cdot xLi_3V_2(PO_4)_3/C$ at 0.1 C.

Fig. 4 shows the initial charge and discharge profiles of the $(1-x)LiFePO_4 \cdot xLi_3V_2(PO_4)_3/C$ (x=0, 0.1, 0.2, 0.3, 0.4, 0.5, and 1) materials between 2.5 and 4.3 V at the rate of 0.1 C at room temperature. For the sample where x=0 corresponding to $LiFePO_4/C$, a long reversible voltage plateau around 3.45 V is observed, corresponding to the phase transition from $LiFePO_4$ to $FePO_4$. The initial discharge capacity of the $LiFePO_4/C$ cathode is 141.5 $mAh \cdot g^{-1}$. For the sample where

New Journal of Chemistry Accepted Manuscript

x=1 ($Li_3V_2(PO_4)_3$/C), three subsequent plateaus appear during the charging process around 3.6, 3.7, and 4.1 V, corresponding to the extraction of the first two Li^+ ions from $Li_3V_2(PO_4)_3$/C [31,44]. The initial discharge capacity of $Li_3V_2(PO_4)_3$/C cathode is 123.7 $mAh \cdot g^{-1}$. For the samples where x=0.1, 0.2, 0.3, 0.4, and 0.5, the (1-x)$LiFePO_4 \cdot xLi_3V_2(PO_4)_3$/C composites exhibit four plateaus corresponding to both $LiFePO_4$/C and $Li_3V_2(PO_4)_3$/C. The discharge capacity increases rapidly from x=0 to x=0.2. However, when $x \geqslant 0.3$, the discharge capacity of the materials decreases, but is still higher than the capacity of pristine $Li_3V_2(PO_4)_3$/C. This phenomenon may be attributed to the fact that the actual specific capacity of $Li_3V_2(PO_4)_3$ is lower than that of $LiFePO_4$[45]. When $x \geqslant 0.3$, the width of the plateau at 3.45 V becomes shorter, owing to the decrease in the amount of $LiFePO_4$ with increase in the vanadium content, and the plateaus corresponding to $Li_3V_2(PO_4)_3$ and $LiFePO_4$ merge to produce a fairly smooth curve. Note that the $0.8LiFePO_4 \cdot 0.2Li_3V_2(PO_4)_3$/C composite exhibits the highest discharge capacity of 158.7 $mAh \cdot g^{-1}$, which is higher than that of pure $LiFePO_4$/C and other vanadium alloyed samples.

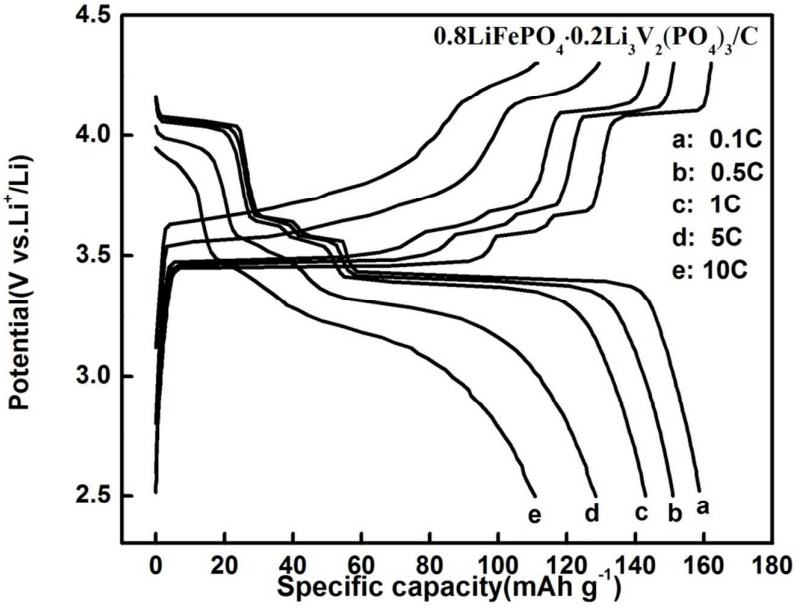

Fig. 5 Charge and discharge curves of of $0.8LiFePO_4 \cdot 0.2Li_3V_2(PO_4)_3$/C at various rates.

New Journal of Chemistry Accepted Manuscript

The charge and discharge profiles of $0.8LiFePO_4 \cdot 0.2Li_3V_2(PO_4)_3/C$ measured at various rates with cut off voltage between 2.5 and 4.3 V are shown in Fig. 5. The $0.8LiFePO_4 \cdot 0.2Li_3V_2(PO_4)_3/C$ composite delivers an initial discharge capacity of 158.7 $mAh \cdot g^{-1}$ at 0.1 C. Even with increase in the current rate to 5 C and 10 C, the capacity still remains at 125.8 and 110.8 $mAh \cdot g^{-1}$, respectively. The charge and discharge curves demonstrate that the improved properties are likely a result of compositing with $Li_3V_2(PO_4)_3$.

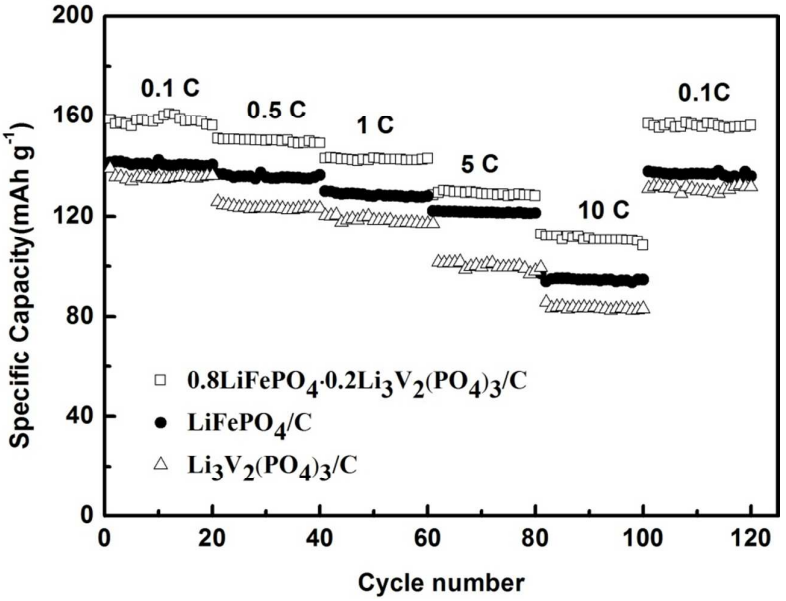

Fig. 6 Cycle performance of samples at different discharge rates.

Fig. 6 shows the cycle performances of the $LiFePO_4/C$, $Li_3V_2(PO_4)_3/C$, and $0.8LiFePO_4 \cdot 0.2Li_3V_2(PO_4)_3/C$ composites at different rates, namely 0.1 C, 0.5 C, 1 C, 5 C, and 10 C. The cycle performance of $0.8LiFePO_4 \cdot 0.2Li_3V_2(PO_4)_3/C$ is observed to be much better than those of $LiFePO_4/C$ and $Li_3V_2(PO_4)_3/C$, both at the low discharge rate of 0.1 C as well as at the high rate of 10 C. At the discharge rate of 10 C, $0.8LiFePO_4 \cdot 0.2Li_3V_2(PO_4)_3/C$ exhibits an excellent capacity of 112.8 $mAh \cdot g^{-1}$, whereas $LiFePO_4/C$ and $Li_3V_2(PO_4)_3/C$ show low capacities of 99.4 and 97.2 $mAh \cdot g^{-1}$, respectively. In addition, $0.8LiFePO_4 \cdot 0.2Li_3V_2(PO_4)_3/C$ shows a lower degree of

New Journal of Chemistry Accepted Manuscript

polarization than $LiFePO_4$/C and $Li_3V_2(PO_4)_3$/C, especially at high rates. This also explains why $0.8LiFePO_4 \cdot 0.2Li_3V_2(PO_4)_3$/C shows better electrochemical performance. Moreover, when the current density is reverted to 0.1 C from 10 C, the discharge capacity of $0.8LiFePO_4 \cdot 0.2Li_3V_2(PO_4)_3$/C returns to 156.9 $mAh \cdot g^{-1}$, illustrating that the structure of $0.8LiFePO_4 \cdot 0.2Li_3V_2(PO_4)_3$/C remains stable after cycling. The improvement in cyclability is likely also attributable to the inclusion of vanadium.

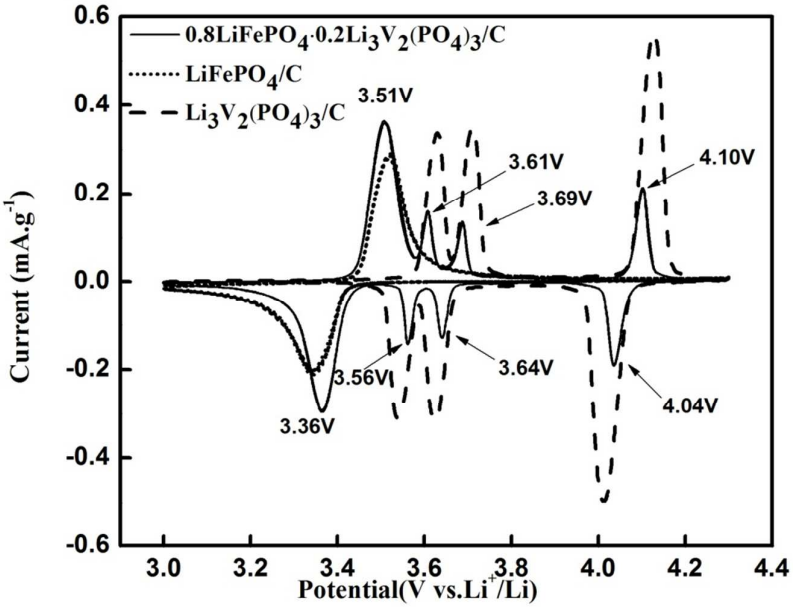

Fig. 7 CV curves of samples at a sweep rate of 0.1 $mV \cdot s^{-1}$ between 3.0-4.3V.

The CV curves of $LiFePO_4$/C, $Li_3V_2(PO_4)_3$/C, and $0.8LiFePO_4 \cdot 0.2Li_3V_2(PO_4)_3$/C in voltage range of 3.0-4.3 V are shown in Fig. 7. In the case of $LiFePO_4$/C, only one pair of redox peaks around 3.52 and 3.34 V is ascribed to the Fe^{2+}/Fe^{3+} potential. Meanwhile, the $Li_3V_2(PO_4)_3$/C samples exhibit three anodic peaks around 3.63, 3.71, and 4.13 V and three cathodic peaks around 3.54, 3.63, and 4.01 V corresponding to the V^{4+}/V^{3+} redox pair. On the other hand, there are four pairs of redox peaks in the CV curves of $0.8LiFePO_4 \cdot 0.2Li_3V_2(PO_4)_3$/C, consisting of both the redox peaks of $LiFePO_4$/C as well as $Li_3V_2(PO_4)_3$/C. The CV data are in good agreement with the

New Journal of Chemistry Accepted Manuscript

charge and discharge curves. The interval between the anodic and cathodic peaks of $0.8LiFePO_4 \cdot 0.2Li_3V_2(PO_4)_3/C$ is smaller than those for pristine $LiFePO_4/C$ and $Li_3V_2(PO_4)_3/C$. This result indicates that the electrochemical reversibility and lithium ion diffusion of $LiFePO_4/C$ is improved by the addition of $Li_3V_2(PO_4)_3$. Meanwhile, electrode polarization is reduced, which results in enhanced electrochemical properties [31].

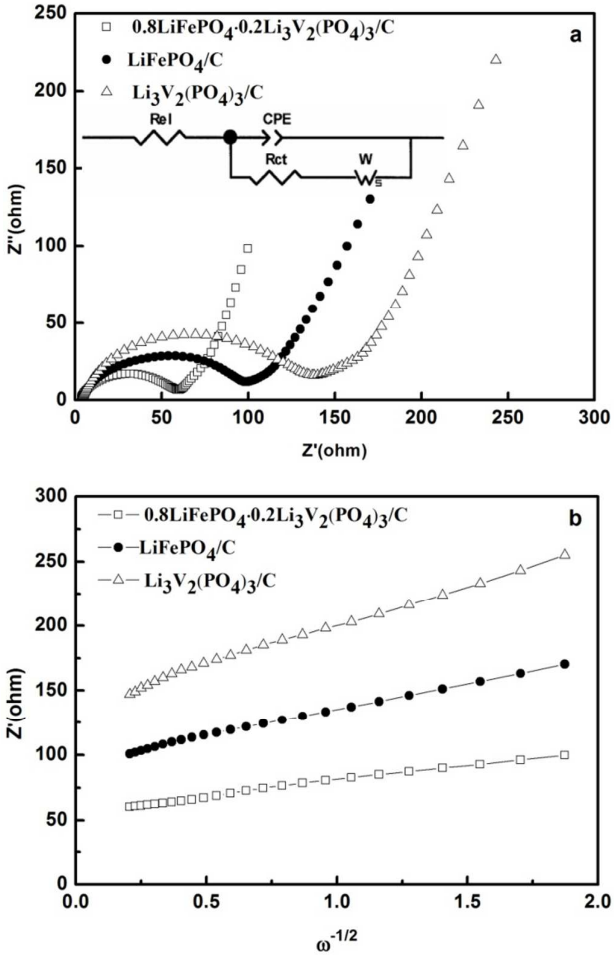

Fig. 8(a) Nyquist plots of samples; (b) the relationship between Z' and $\omega^{-1/2}$.

Table 2

Calculated electrochemical parameters from ac impedance spectra of samples using Z-view software

New Journal of Chemistry Accepted Manuscript

Sample	$R_{el}(\Omega)$	$R_{ct}(\Omega)$	$W_s(\Omega)$	$D_{Li+}(cm^2s^{-1})$
$Li_3V_2(PO_4)_3/C$	4.75	64.8	120.2	$9.91*10^{-16}$
$LiFePO_4/C$	5.01	139.7	83.4	$2.26*10^{-15}$
$0.8LiFePO_4 \cdot 0.2Li_3V_2(PO_4)_3/C$	4.73	58.3	44.4	$6.31*10^{-15}$

R_{el} represents electrolyte resistance, R_{ct} represents the charge-transfer resistance, W_s represents the Warburg impedance, D_{Li+} represents Li^+ transfer coefficient.

Fig. 8a presents the Nyquist plots of samples $LiFePO_4/C$, $Li_3V_2(PO_4)_3/C$, and $0.8LiFePO_4 \cdot 0.2Li_3V_2(PO_4)_3/C$ in the frequency range of 1 Hz to 100 kHz, which are measured at the charged state of 4.5 V after initial cycle at 0.1 C. The equivalent is also provided. The EIS spectra in all the three cases are composed of a semicircle in the high frequency range and an inclined line in the low frequency range. The equivalent circuit is also shown in Fig. 8a. The semicircle is attributed to the charge transfer process and the diameter of the semicircle is approximately equal to the charge transfer resistance (R_{ct}) [46]. The inclined line may be modeled using the Warburg impedance, W_s, which arises from the Li^+ diffusion in the electrode [47]. The model also contains a constant phase element. The EIS values obtained by the equivalent circuit simulation and the diffusion coefficients of lithium ion are listed in Table 2. The values of R_{ct} and W_s for $0.8LiFePO_4 \cdot 0.2Li_3V_2(PO_4)_3/C$ are much lower than those for $LiFePO_4/C$ and $Li_3V_2(PO_4)_3/C$, indicating higher electronic conductivity and Li^+ diffusion coefficient better electrochemical performance. This further confirms that the addition of $Li_3V_2(PO_4)_3$ to $LiFePO_4$ can improve the electrical conductivity and enhance reaction kinetics [31].

Fig. 8b shows the relationship between Z' and squarer root of frequency ($\omega^{-1/2}$) in the low frequency region. A linear characteristic could be seen for every curve. The diffusion coefficients of lithium ion are shown in Table 2. The lithium ion diffusion coefficient is calculated according to the following equation [37, 48-49]:

$$D = (0.5\, R^2\, T^2)/(A^2\, n^4\, F^4\, C^2\, \sigma^2) \qquad (1)$$

Where D is the Li^+ diffusion coefficient, R is the gas constant T is the absolute

New Journal of Chemistry Accepted Manuscript

temperature, A is the surface area of the electrode, n is the number of electrons per molecule during oxidization, F is the Faraday's constant, C is the molar concentration of Li+, σ is the Warburg factor which is relative with Z':

$$Z' = R_{el} + R_{ct} + \sigma\,\omega^{-1/2} \quad (2)$$

The lithium ion diffusion coefficient of $0.8LiFePO_4 \cdot 0.2Li_3V_2(PO_4)_3/C$ is higher than those of $LiFePO_4/C$ and $Li_3V_2(PO_4)_3/C$. This result is in agreement with that the high rate performance of $0.8LiFePO_4 \cdot 0.2Li_3V_2(PO_4)_3/C$ composite.

Conclusion

In this study, $(1-x)LiFePO_4 \cdot xLi_3V_2(PO_4)_3/C$ (x=0, 0.1, 0.2, 0.3, 0.4, 0.5, and 1) composite cathode materials were synthesized by a new sol-gel method. H_2O_2 was used to dissolve V_2O_5 to form V_2O_5 hydrogels and decrease the particle size of V_2O_5. Meanwhile, DMF formed complexes with the metal ions and slowed the release of the metal ions, whereas the addition of H_3PO_4 controlled the particle size. XRD patterns of $(1-x)LiFePO_4 \cdot xLi_3V_2(PO_4)_3/C$ were composed of peaks corresponding to the $LiFePO_4/C$ and $Li_3V_2(PO_4)_3/C$ phases without any impurities. The performance of the $0.8LiFePO_4 \cdot 0.2Li_3V_2(PO_4)_3/C$ sample is much improved compared to the other composites, with particle size in the range of 30-50 nm, high specific capacity, and excellent cycling stability. This sample delivered an initial discharge capacity of 158.7 $mAh \cdot g^{-1}$ at 0.1 C in the voltage range of 2.5-4.3 V. Even at high rates of 5 C and 10 C, the capacity of $0.8LiFePO_4 \cdot 0.2Li_3V_2(PO_4)_3/C$ was retained at 125.8 and 110.8 $mAh \cdot g^{-1}$, respectively. While on one hand, the conductive carbon wrapping on the $(1-x)LiFePO_4 \cdot xLi_3V_2(PO_4)_3/C$ particles enhanced the conductivity of the electrode, on the other hand, the incorporation of $Li_3V_2(PO_4)_3$ enhanced the Li^+ diffusion speed and electronic conductivity of $LiFePO_4$-based materials. Based on the results of this study, the electrochemical properties of $(1-x)LiFePO_4 \cdot xLi_3V_2(PO_4)_3/C$ can be improved through further investigations. These polyanion $(1-x)LiFePO_4 \cdot xLi_3V_2(PO_4)_3/C$ cathode materials with excellent rate capability and long cycle life can be able to use in electric vehicle and other high power density applications in the future.

New Journal of Chemistry Accepted Manuscript

Acknowledgements

This study was supported by the National Natural Science Foundation of China (№ 21061015) and (№ 21263021).

References

[1] Y.C. Lin, G.T.K. Fey, P.J. Wu, J.K. Chang, H.M. Kao, *J. Power Sources* 2013, **244**, 63-71.

[2] T. Masese, Y. Orikasa, T. Mori, K. Yamamoto, T. Ina, T. Minato, *Solid State Ionics* 2014, **262**, 110-114.

[3] P.Y. Zhai, S.X. Zhao, H.M. Cheng, *Electrochim. Acta* 2015, **153**, 217-224.

[4] A.K. Padhi, K.S. Nanjundaswamy, C. Masquelier, S. Okada & J.B. Goodenough, *J. Electrochem. Soc.* 1997, **144**, 1609-1613.

[5] X.C. Wang, Y.D. Huang, D.Z Jia, Z.P. Guo, D. Ni, *J. Solid State Electroche.* 2012, **16** (1), 17-24.

[6] C.B. Zhu, X.K. Mu, J. Popovic, K. Weichert, P.A. Aken, Y. Yu, *Nano lett*. 2014, **14** (9), 5342-5349.

[7] M. Filkusová, A. Fedorková, R. Oriňáková, *New Carbon Mater*, 2013, **28** (1), 1-7.

[8] Y. Liu, C. Cao, J. Li, *Electrochim. Acta* 2010, **55** (12), 3921-3926.

[9] Y.H. Huang, J.B. Goodenough, *Chem. Mater.* 2008, **20** (23), 7237-7241.

[10] A. Yamada, S.C. Chung, K. Hinokuma. *J. Electroche. Soc.* 2001, **148** (3), A224-A229.

[11] Y.G. Huang, F. H. Zheng, X.H. Zhang, Y.H. Li, J.C. Yin, Q.Y. Li, *Solid State Ionics*, 2013, **249**, 158-164.

[12] X. He, J. Li, Y. Cai, J.R. Ying. *J. power sources* 2005, **150**, 216-222.

[13] R. Malik, D. Burch and M. Bazant, *Nano let.* 2010, **10**(10), 4123-4127.

[14] N. Hua, C. Y. Wang, X. Kang, T. Wumair, Y. Han, *J. Alloys Compd.* 2010, **503** (1), 204-208.

[15] H.C. Shin, S.B Park, H. Jang, *Electrochim. Acta* 2008, **53** (27), 7946-7951.

[16] Y.J. Zhong, J.T. Li, Z.G. Wu, X.D. Guo, B.H. Zhong, S.G. Sun, *J. Power*

New Journal of Chemistry Accepted Manuscript

Sources 2013, **234**, 217-222.

[17] Z.H. Wang, L.X. Yuan, W.X. Zhang, Y.H. Huang, *J. Alloys Compd.* 2012, **532**, 25-30.

[18] M.M. Ren, Z. Zhou, X.P. Gao, W.X. Peng, J.P. Wei, *J. Phys. Chem. C* 2008, **112** (14), 5689-5693.

[19] J. Gaubicher, C. Wurm, G. Goward, C. Masquelier, L. Nazar, *Chem. Mater*. 2000, **12** (11), 3240-3242.

[20] Y. P. Xi, Y.H. Zhang, Z. Su. *J. Alloys Compd*. 2015, **628**, 396-400.

[21] J.W. Wang, J. Liu, G.L. Yang, X.F. Zhang, X.D. Yan, X.M. Pan, R.S. Wang, *Electrochim. Acta* 2009, **54** (26), 6451-6454.

[22] A. Pan, J. Liu, J.G. Zhang, *Electrochem. Commun*. 2010, **12** (12), 1674-1677.

[23] Y.Q. Qiao, X.L. Wang, Y.J. Mai, *J. Power Sources* 2011, **196** (20), 8706-8709.

[24] M.R. Yang, W.H. Ke, S.H. Wu, *J. Power Sources* 2007, **165** (2), 646-650.

[25] J. Ma, B.H. Li, H.D. Du, C.J. Xu, F.Y. Kang, *J. Electrochem. Soc.* 2011, **158** (1), A26-A32.

[26] X.P. Zhang, H.J. Guo, X.H. Li, Z.X. Wang, L. Wu, *Solid State Ionics* 2012, **212**, 106-111.

[27] J.C. Zheng, X.H. Li, Z.X. Wang, S.S. Niu, D.R. Liu, L. Wu, L.J. Li, *J. Power Sources* 2010, **195** (9), 2935-2938.

[28] X.H. Rui, N. Ding, J. Liu, C. Li, C.H. Chen, *Electrochim. Acta* 2010, **55** (7), 2384-2390.

[29] N. Zouari, M.B. Amor, T. Mhiri, *J. alloys compd*. 1996, **240** (1), 70-75.

[30] L.L. Zhang, G. Liang, A. Ignatov, M.C. Croft, *J. Phys. Chem. C* 2011, **115** (27), 13520-13527.

[31] J.Y. Xiang, J.P. Tu, L. Zhang, X.L. Wang, Y. Zhou, Y.Q. Qiao, Y. Lu, *J. Power Sources* 2010, 195(24), 8331-8335.

[32] J.C. Zheng, X.H. Li, Z.X. Wang, J.H. Li, L.J. Li, L. Wu, H.J. Guo, *Ionics* 2009, **15** (6), 753-759.

[33] L. Wu, J.J. Lu, S. Zhong, *J. Solid State Electrochem.* 2013, 17 (8), 2235-2241.

New Journal of Chemistry Accepted Manuscript

[34] L. Wu, J.J. Lu, G. Wei, P.F. Wang, H. Ding, J.W. Zheng, X.W. Li, S.K. Zhong, *Electrochim. Acta* 2014, **146**, 288-294.

[35] L.N. Wang, Z.C. Li, H.J. Xu, *J. Phys. Chem. C* 2008, **112** (1), 308-312.

[36] G. Yang, C.Y. Jiang, X.M. He, *Ionics* 2013, **19** (9), 1247-1253.

[37] C. Gao, H. Liu, G.B. Liu, J. Zhang, W. Wang, *Mater. Sci. and Eng. B.* 2013, 178, 272-276

[38] S.S. Li, Z. Su, X.K. Jiang, *Mater. Lett*. 2015.

[39] Y. Guo, Y.D. Huang, D.Z. Jia, X.C. Wang, N. Sharma, Z.P. Guo, X.C. Tang, *J. Power Sources* 2014, **246**, 912-917.

[40] S.K. Zhong, L. Wu, J.Q. Liu. *Electrochim. Acta* 2012, **74**, 8-15.

[41] J. Mendialdua, R. Casanova, Y. Barbaux, *J. Electron Spectrosc. Relat. Phenom.* 1995, **71**, 249-261.

[42] Q.Q. Chen, J.M. Wang, Z. Tang, W.C. He, H.B. Shao, J.Q. Zhang, *Electrochim. Acta* 2007, **52**, 5251-5257.

[43] S.T. Myung, S. Komaba, N. Hirosaki, H. Yashiro, N. Kumagai, *Electrochim. Acta* 2004, **49**, 4213-4222.

[44] F. Wang, J. Yang, Y. Nuli, J.L. Wang, *Electrochim. Acta* 2013, **103**, 96-102.

[45] X.J. Chen, G.S. Cao, X.B. Zhao, J.P. Tu, T.J. Zhu, *J. Alloys Compd.* 2008, **463** (1), 385-389.

[46] S.K. Liu, J. Xu, D.Z. Li, Y. Hu, X. Liu, K. Xie, *J. Power Sources* 2013, **232**, 258-263.

[47] T. Ma, A. Muslim, Z. Su, *J. Power Sources* 2015, **282**, 95-99.

[48] M.S. Zhao, G.L. Huang, W.G. Zhang, H.Y. Zhang, X.P. Song, *Amer. Chem. Soc.* 2013, **27**, 1162-1167.

[49] X.P. Zhang, H.J. Guo, X.H. Li, Z.X. Wang, L. Wu, *Solid State Ionics* 2012, **212**, 106-111.

New Journal of Chemistry Accepted Manuscript

Figure Captions

Fig. 1 XRD patterns of (1-x)$LiFePO_4 \cdot xLi_3V_2(PO_4)_3$/C samples.

Fig. 2 TEM and HRTEM images of (a)(d) $LiFePO_4$/C, (b)(e) $Li_3V_2(PO_4)_3$/C and (c)(f) $0.8LiFePO_4 \cdot 0.2Li_3V_2(PO_4)_3$/C.

Fig. 3 XPS spectra of V2p (a) and Fe2p (b) in $0.8LiFePO_4 \cdot 0.2Li_3V_2(PO_4)_3$/C.

Fig. 4 Initial charge-discharge curves of (1-x)$LiFePO_4 \cdot xLi_3V_2(PO_4)_3$/C at 0.1 C.

Fig.5 Charge and discharge curves of of $0.8LiFePO_4 \cdot 0.2Li_3V_2(PO_4)_3$/C at various rates.

Fig. 6 Cycle performance of samples at different discharge rates.

Fig.7 CV curves of samples at a sweep rate of 0.1 $mV \cdot s^{-1}$ between 3.0-4.3V.

Fig. 8(a) Nyquist plots of samples; (b) the relationship between Z' and $\omega^{-1/2}$.

New Journal of Chemistry Accepted Manuscript

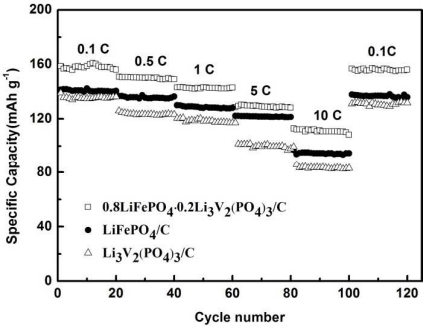

$0.8LiFePO_4 \cdot 0.2Li_3V_2(PO_4)_3/C$ were synthesized by new sol-gel method, which delivered an initial discharge capacity of 158.7 $mAh \cdot g^{-1}$ at 0.1 C.

New Journal of Chemistry Accepted Manuscript